Nanoscale

Accepted Manuscript

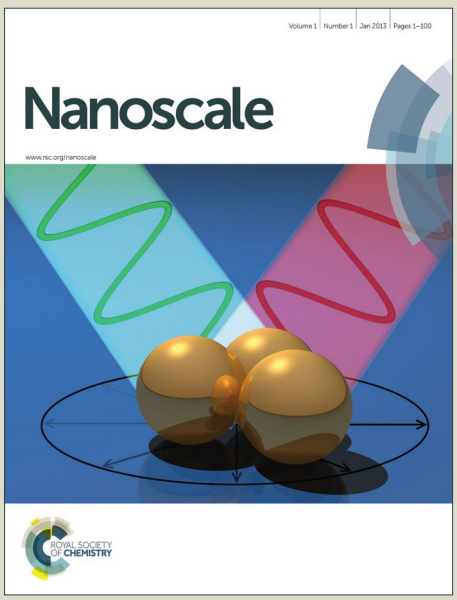

ROYAL SOCIETY OF CHEMISTRY

www.rsc.org/nanoscale

Ultratrace Level Determination and Quantitative Analysis of Kidney Injury Biomarkers in Patient Samples Attained by Zinc Oxide Nanorods

Manpreet Singh[†], *Anginelle Alabanza*[†], Lorelis E. Gonzalez [†], *Weiwei Wang*[‡], *W. Brian Reeves*[‡], *and Jong-in Hahm*[†,*]

[†]*Department of Chemistry, Georgetown University, 37th & O Sts. NW., Washington, DC 20057.*

[‡]*Division of Nephrology, The Penn State College of Medicine, Milton S. Hershey Medical Center, Hershey, Pennsylvania 17033.*

**Address Correspondence to jh583@georgetown.edu*

ABSTRACT

Determining ultratrace amounts of protein biomarkers in patient samples in a straightforward and quantitative manner is extremely important for early disease diagnosis and treatment. Here, we successfully demonstrate the novel use of zinc oxide nanorods (ZnO NRs) in the ultrasensitive and quantitative detection of two acute kidney injury (AKI)-related protein biomarkers, tumor necrosis factor (TNF)-α and interleukin (IL)-8, directly from patient samples. We first validate the ZnO NRs-based IL-8 results via comparison with those obtained from using a conventional enzyme-linked immunosorbent method in samples from 38 individuals. We further assess the full detection capability of the ZnO NRs-based technique by quantifying TNF-α, whose levels in human urine are often below the detection limits of conventional methods. Using the ZnO NR platforms, we determine the TNF-α concentrations of all 46 patient samples tested, down to the fg/mL level. Subsequently, we screen for TNF-α levels in approximately 50 additional samples collected from different patient groups in order to demonstrate a potential use of the ZnO NRs-based assay in assessing cytokine levels useful for further clinical monitoring. Our research efforts demonstrate that ZnO NRs can be straightforwardly employed in the rapid, ultrasensitive, quantitative, and simultaneous detection of multiple AKI-related biomarkers directly in patient urine samples, providing an unparalleled detection capability beyond those of conventional analysis methods. Additional key advantages of the ZnO NRs-based approach include a fast detection speed, low-volume assay condition, multiplexing ability, and easy automation/integration capability to existing fluorescence instrumentation. Therefore, we anticipate that our ZnO NRs-based detection method will be highly beneficial for overcoming the frequent challenges in early biomarker development and treatment assessment, pertaining to the facile and ultrasensitive quantification of hard-to-trace biomolecules.

Introduction

Cytokines and a subgroup of chemoattractant cytokines known as chemokines are signaling proteins produced by many cells such as neutrophils, monocytes, macrophages, and T-cells.[1-5] Cytokines and chemokines regulate immune responses and are known as important biomarkers of inflammatory diseases. Hence, they are widely used to track and predict disease progressions as well as to monitor patient treatment outcomes.[6-9] One such example is acute kidney injury (AKI), a common disorder with high morbidity and mortality rates in the hospital setting whose biomarkers include various cytokines and chemokines such as interleukins (ILs) and tumor necrosis factors (TNFs).[8-12]

The potentially decisive diagnostic importance of cytokine and chemokine biomarkers continues to drive new assay development.[13-15] The most common methods of detecting cytokines rely on enzyme-linked immunosorbent assays (ELISAs).[3,16,17] Yet, such traditional diagnostic procedures widely employed for the measurement of biomarkers tend to require long assay times and extensive workflows. In addition, these standard methods are often limited to measuring a single type of protein per run. Moreover, typical detection sensitivities of conventional ELISA assays may be insufficient to discern biologically significant perturbations in weakly expressed cytokines. To overcome these challenges, approaches such as microsphere-based assays[18,19] and polymerase chain reaction (PCR)-based assays[20,21] have been developed. For example, previous studies have used bioluminescent proteins as alternative labeling sources to reduce autofluorescence and to permit IL-6 and IL-8 detection in the low pg/mL range.[22] Immuno-PCR methods, generally employing single DNA-coupled antibodies whose signals are amplified with additional steps such as rolling cycle amplification, have yielded a detection range of less than 10 pg/mL for many cytokines.[23] Electroluminescence and square-wave voltammetry methods have also been used to measure TNF-α levels in the range of 3~7 pg/mL.[24] Surface plasmon resonance (SPR) and local surface plasmon resonance (LSPR) effects have been more recently exploited for cytokine measurements as well. The lowest concentration levels of IL-1β and TNF-α in physiologically relevant samples tested with a SPR-based sensor have been reported to be in the 1 ng/mL range[25] and further improved to ~50 pg/mL with the addition of Au nanoparticles for signal

amplification.[26] An optical fiber sensor coupled with Au nanoparticles for LSPR can detect IL-1β of concentrations as low as several tens of pg/mL.[27] These and the wealth of other studies in the literature underscore the significance of cytokines and chemokines in both basic biological and biomedical research as well as the high demand for achieving ultrasensitive detection limits (DLs) of these biomarker proteins in more applied clinical contexts.

The levels of disease-implicated cytokines and chemokines in humans are often well below the tens of pg/mL range which is the customary DLs of conventional techniques. Accordingly, there is a great interest in reducing the lower limits of detection down to the fg/mL range. In particular, the ever-growing need for early diagnosis and treatment in AKI and other cytokine-implicated diseases further warrants an innovative detection means capable of reaching even lower DLs than those currently offered. In this context, we have shown that ZnO NRs permit enhanced detection of fluorescence signals emitted by biomolecules in the form of custom-prepared oligonucleotide constructs and highly purified single-composition proteins in simple media.[28-33]

In this study, we quantify TNF-α and IL-8, two AKI-related biomarkers, in urine samples obtained from patients at risk for AKI by using ZnO NR platforms in fluorescence-based assays. We demonstrate that ultralow amounts of the biomarker proteins can be quantified rapidly and simultaneously in biologically complex, clinical samples using the newly developed ZnO NR fluorescence assay platform. Furthermore, we compare the biomarker readings determined using the ZnO NR platform with the results obtained using a conventional ELISA-based assay on the same patient samples. We determine that the ZnO NR platform can quantify TNF-α and IL-8 levels in urine down to the concentration range of several fg/mL. Lastly, we assess the feasibility of our ZnO NRs-based approach to distinguish between different patient groups to serve as a guide in clinical monitoring. Our efforts presented in this study verify that the exquisite levels of detection for urine cytokines can be conveniently and straightforwardly achieved from minimally processed patient samples, well beyond the detection limits of other standard techniques. Hence, exciting future applications of the ZnO NRs-

based assay schemes are envisaged both in basic biology research and clinical biomarker studies by accommodating other protein systems.

Experimental Methods

ZnO NR Platform Synthesis. The ZnO NR platforms employed for the chemokine and cytokine assays were fabricated by synthesizing vertically oriented ZnO NRs atop a Si substrate in a preconfigured square array pattern. A gas phase synthesis was performed in a home-built chemical vapor deposition reactor, similar to the previously described procedures.[28-31,34-39] Briefly, the Si substrate was prepatterned by microcontact printing 20 nm Au colloidal catalysts (Ted Pella, Inc.; Redding, CA) using an elastomeric poly(dimethylsiloxane) stamp containing periodic square features with side lengths of 10 μm. Subsequent growth of ZnO NRs was carried out by heating a 2:1 by weight mixture of zinc oxide (99.999% purity; Alfa Aesar Inc.) and graphite (99.99% purity; Alfa Aesar, Inc) to 950 °C for 1 h under a constant Ar gas flow.

Preparation of the Proteins and Antibodies. Unlabeled monoclonal anti-human IL-8 (clone 6217, R&D Systems) and TNF-α (clone 6401, R&D Systems) antibodies were used as the primary capture antibodies in the duplexed sandwich assay. Recombinant human IL-8 and TNF-α (R&D Systems), were reconstituted in deionized water (DI) to a concentration of 2 ng/mL and 10 ng/mL, respectively, and stored in small aliquots at -70 °C until use. IL-8 and TNF-α calibration standards were prepared fresh each assay day by serial dilution of the human IL-8 and TNF-α to the following concentrations: 1000, 100, 10, 1, 0.1, 0.01, and 0.001 pg/mL in phosphate-buffered saline (PBS). Lyophilized bovine serum albumin (BSA) was purchased from VWR Scientific, Inc. (West Chester, PA) and reconstituted and diluted per manufacturing recommendations in PBS. Polyclonal human TNF-α (AB 210-NA, R & D Systems) and IL-8 (AB 208-NA, R & D Systems) antibodies were labeled with Alexa 488 and Alexa 546, respectively, using the Monoclonal Antibody Labeling kit (Invitrogen Molecular Probes, Eugene,

OR) following manufacturer's instructions. After labeling, the unreactive, free dye was removed by gel filtration. Post-filtration, the final protein concentration and degree of labeling (DOL) were determined spectrophotometrically using 280 nm, 494 nm, and 554 nm wavelengths for the proteins, Alexa 488-labeled TNF-α, and Alexa 546-labeled IL-8, respectively. The labeled antibody yields were generally 60-80% with 7-9 molecules of dye/molecule of antibody DOL.

Urine Sample Collection. Urine samples were collected from patients admitted to the medical intensive care unit (ICU) of the Penn State Hershey Medical Center. After obtaining informed consent, and within the first 24 h of ICU admission, a urine sample was obtained as either a freely voided specimen or was collected from an indwelling urine drainage system. Urine samples were placed on ice if processing was not performed within 30 min of sample collection. Urine was processed by centrifugation at 3000 g for 10 min at 4 ^{o}C. One mL aliquots of the supernatant urine were transferred into cryovials and stored at -70 ^{o}C until used for the cytokine assays. Clinical and laboratory information was abstracted from the patient record including results of serum creatinine measurements, which were typically measured at least once daily. The diagnosis of AKI was made based on changes in serum creatinine levels using the Acute Kidney Injury Network criteria.[40] All procedures involving human subjects were approved by the Institutional Review Board of the Penn State College of Medicine.

Sandwich Protein Assays on ZnO NRs. Prior to performing the duplexed cytokine assays on the ZnO NR platforms, the as-grown NRs were first cleaned by rinsing thoroughly with ethanol and DI followed by drying with N_2 gas. For the first step, a 15 μL aliquot of a 1:1 mixture of 1 μg/mL TNF-α and 1 μg/mL IL-8 unlabeled primary antibodies was deposited on the ZnO NR platform for 15 min. This and subsequent incubation steps of the sandwich assay on the ZnO NR platform were conducted inside a humidity-controlled chamber at room temperature and protected from light. The ZnO NR platform was then thoroughly rinsed using 40 μL aliquots of PBS and subjected to blocking by incubation with 15 μL of 5 μg/mL BSA for 15 minutes. Post-passivation, the ZnO NR platform was again amply rinsed with

40 μL aliquots of DI. Then, a 15 μL volume of either a 1:1 mixture of TNF-α and IL-8 calibration standards or a 1:5 dilution of human urine samples in PBS was deposited onto the platform. After 15 min incubation with standards of known concentrations or patient samples of unknown concentration, the platform was rinsed with DI thoroughly and lastly incubated with 15 μL of a 1:1 mixture of 1.5 μg/mL Alexa 488-labeled TNF and 1.5 μg/mL Alexa 546-labeled IL-8 antibodies for 30 min. Post incubation with the labeled antibodies, the platform was rinsed amply with DI and dried gently under a stream of N_2 gas before immediately being imaged for fluorescence. For regenerating the ZnO NR platform after the fluorescence detection, the biomolecules and residual fluorescence were removed by exposing the ZnO NR platform to N_2 plasma for 5 min under vacuum in a Harrick PDC-32G plasma cleaner at a setting of 18 W radio frequency followed by thorough rinsing in ethanol and then DI.

ELISA Assays. TNF-α and IL-8 were measured in the same urine samples using commercially available ELISA kits (Quantikine IL-8/CXCL8 kit and Quantikine TNF-α kit, R and D Systems, Minneapolis, MN) per manufacturers' protocols. All assays were performed in duplicate. After color development, the absorbance at 450 nm wavelength was determined using a plate reading spectrophotometer. The absorbance values for the standards were fit using a 4-parameter polynomial regression (Origin9, Origin Labs) which was then used to calculate the concentrations of the unknown patient samples.

ZnO NR Characterization, Fluorescence Measurements, and Data Analysis. For morphological and structural characterization, as-grown ZnO NRs were evaluated and imaged using a FEI/Philips XL 20 scanning electron microscope (SEM) operating at 20 kV. All optical measurements for the ZnO NRs-based assays were conducted using a Zeiss Axio Imager A2M microscope (Carl Zeiss, Inc., Thornwood, NY) equipped with an AxioCAM HRm digital camera. The reflected bright-field illumination and unpolarized fluorescence excitation were produced by a 12 V/100 W halogen lamp and 120 W mercury vapor lamp (X-Cite 120Q), respectively. Two different filter modules allowed for the duplexed fluorescence characterization of the green emission from Alexa 488-labeled TNF-α (450-490 nm excitation and 510-540 nm collection) and red emission from Alexa 546-labeled IL-8 (540-552 nm

excitation and 575-640 nm collection). Dichromatic beam splitters operating at 495 nm and 560 nm were also employed to separate the excitation light from the collected biomolecular signal for TNF-α and IL-8, respectively. Images were acquired in a dark room setting using a 2 sec exposure through an EC Epiplan-NEOFLUAR 50x magnification objective lens (numerical aperture, NA = 0.8). Images were analyzed using the processing software AxioVision (Carl Zeiss, Inc), Image J (a Java-based program), and Origin 8 (OriginLab Corp.).

Results and Discussion

TNF-α and IL-8 were selected as model cytokines and chemokines in our study due to their pertinence in the pathophysiology and diagnosis of AKI as well as their typical concentration levels found in urine. The relevance of the TNF-α and IL-8 markers to AKI has been reported in the past.[6-9] In addition to their biomedical relevance, the differences in the typical ranges of TNF-α and IL-8 in urine samples make them ideal to evaluate our ZnO NRs-based detection approach. The typical concentration levels of TNF-α in human urine samples are often below the DLs of conventional cytokine detection platforms.[41] Those of IL-8, on the other hand, typically exhibit values above several tens of pg/mL and well into the ng/mL range,[42,43] which can be determined with traditional techniques. Therefore, we carried out both ELISA- and ZnO NRs-based assays from the same set of patient samples. By performing the two comparative assays of the ELISA- and ZnO NRs-based detection on the same set of patient samples, we first examined whether the IL-8 levels from the highly-expressed samples agree between the two detection methods. Next, we assessed the detection capability of the ZnO NRs in ascertaining those ultralow protein levels of TNF-α in the patient samples that fall below the ELISA DL.

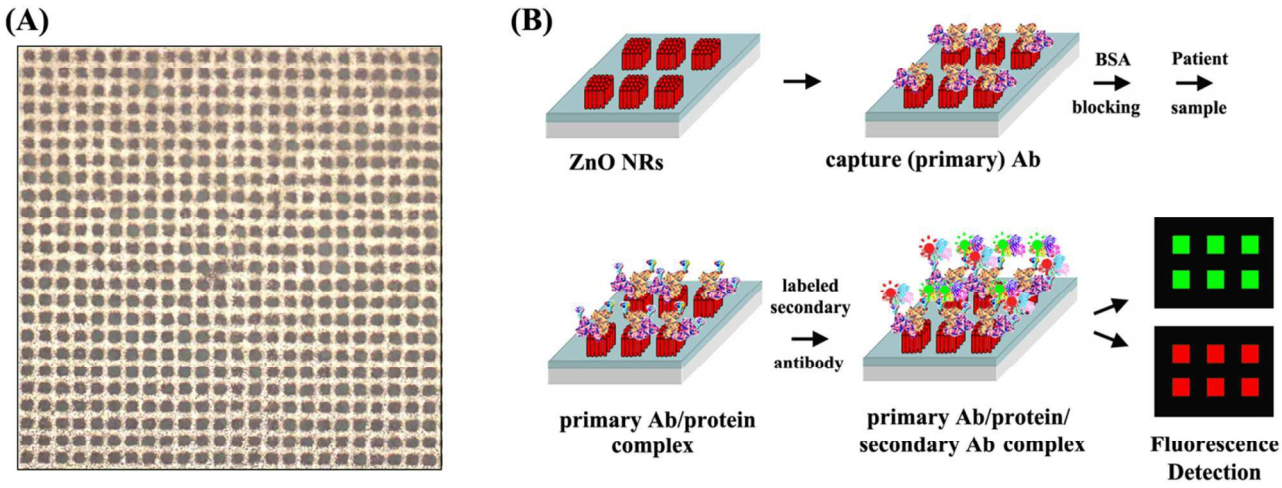

Figure 1. (A) The bright field optical microscope image of a ZnO NR square array displays the typical NR platforms used in the chemokine and cytokine assays. The ZnO NRs were vertically grown on a Si substrate prepatterned with microcontact-printed catalysts into a square array. The view frame corresponds to 0.5 x 0.5 mm^2 in size. **(B)** Overall schematics of the duplexed detection of IL-8 and TNF-α using the ZnO NR platforms are presented. The simultaneous sandwich assay scheme involved primary as well as labelled secondary antibodies targeting either known concentrations of IL-8 and TNF-α to establish calibration curves or patient urine samples to determine the unknown IL-8 and TNF-α amounts in subject individuals.

The assay method is outlined in Fig. 1. Square arrays of vertically grown ZnO NRs were prepared as described in our previous studies[28-31] and further employed directly after their synthesis as the patient cytokine and chemokine detection platforms. The crystal and chemical structures of the as-grown nanomaterials were reported previously along with their X-ray diffraction and photoluminescence data.[44,45] In short, the patterned ZnO NR ensembles were obtained by localizing catalysts only to predetermined locations of the growth substrate via microcontact printing. An optical micrograph of a typical ZnO NR square array produced via the microcontact-printed catalyst delivery method is shown

in Fig. 1(A), presenting a 0.5 x 0.5 mm^2 view frame of the ZnO NR patches. The ZnO NR arrays used in our bioassays contain square blocks of 10 μm in length spaced 10 μm apart. With no post-synthetic modifications, the ZnO NR arrays were employed to carry out the sandwich protein assay, whose key biomedical procedures are depicted step by step in Fig. 1(B). The typical diameters and lengths of the NRs employed in our measurements range from 150 to 300 nm and from 5 to 10 μm, respectively, depending on the array plates. The chosen NR size ranges are known to couple and guide visible light[46,47] and the typical SEM images of these ZnO NRs are provided in ESI, Fig. S1†. The key steps outlined in Fig. 1(B) include the deposition of TNF-α and IL-8 primary antibodies on the NRs, the blocking of any exposed platform surface with bovine serum albumin (BSA), the introduction of either standards of known TNF-α and IL-8 concentrations for obtaining calibration curves or patient urine samples of unknown TNF-α and IL-8 concentrations for evaluating the AKI biomarkers in clinical samples, and subsequent addition of Alexa 488-labeled TNF-α and Alexa 546-labeled IL-8 secondary antibodies. Fluorescence signals arising after the multi-layer protein interactions were obtained by sequentially imaging the samples under the excitation and emission settings appropriate for Alexa 488 and Alexa 546. Representative emission data are qualitatively presented in Fig. 2(A). The TNF-α (left) and IL-8 (right) fluorescence images were obtained from the same assay to demonstrate the multiplexing capability of the platform. As a direct comparison, the panels in Fig. 2(B) display SEM images of the ZnO NR array platform used in the bioassays to show the morphology and dimensions of the individual square patches of vertically oriented ZnO NRs. As evidenced by the fluorescence panel (F) in the inset of the left image in Fig. 2(B), ZnO NRs exhibit no background fluorescence emission upon excitation at the wavelength ranges used to detect the proteins. Although the inset shows the fluorescence panel from ZnO NRs when using the excitation (ex) and collection (col) wavelength ranges of λ_{ex} = 450-490 nm and λ_{col} = 510-540 nm, the absence of background fluorescence from ZnO NRs was also confirmed under other visible wavelength settings commonly employed for biologically relevant fluorescence measurements.

The fluorescence intensities obtained from different patient samples were further quantified. Several examples of the fluorescence readings are shown in Fig. 2(C) for the selected patient samples. In our measurements, all NR square patches in an array were treated with the same patient sample per assay from which eight fluorescence frames were acquired at various platform areas. The fluorescence signals from ~550 NR square patches per sample were subsequently analyzed to attain the average fluorescence intensity as well as the associated error bars reported for each patient sample in Fig. 2(C). The relative amounts of the TNF-α and IL-8 biomarkers present in the individual subjects are represented by the bar graphs of the fluorescence intensities. For example, it can be seen that patient 17 had a comparable urine IL-8 level with the rest of the group, whereas the TNF-α level was lower than the others. The reproducibility of the fluorescence signal in the ZnO NRs-based protein detection method was also assessed by repeating the cytokine and chemokine measurements for two selected patients (17 and 19). For each of these patients, the ZnO NRs-based assays were repeated five times on the same NR plate, and the average fluorescence intensities obtained from these five independent runs per patient are shown in the bar graph sets indicated with ** in Fig. 2(D). In addition, the potential variability in the biomarker detection due to ZnO NR array-to-array differences was also evaluated by assaying the same samples on three different ZnO NR plates. The results are displayed in the paired bar graphs marked with * in Fig. 2(D). The inter-assay (the assessment of ZnO NR plate-to-plate consistency) coefficients of variation for TNF-α and IL-8 were 12 and 2.8 % while the intra-assay (the assessment from repeated measurements on the same ZnO NR plate) coefficients of variation were 16.5 and 2.5 %. Both are below the generally accepted value of 10-20%.[48]

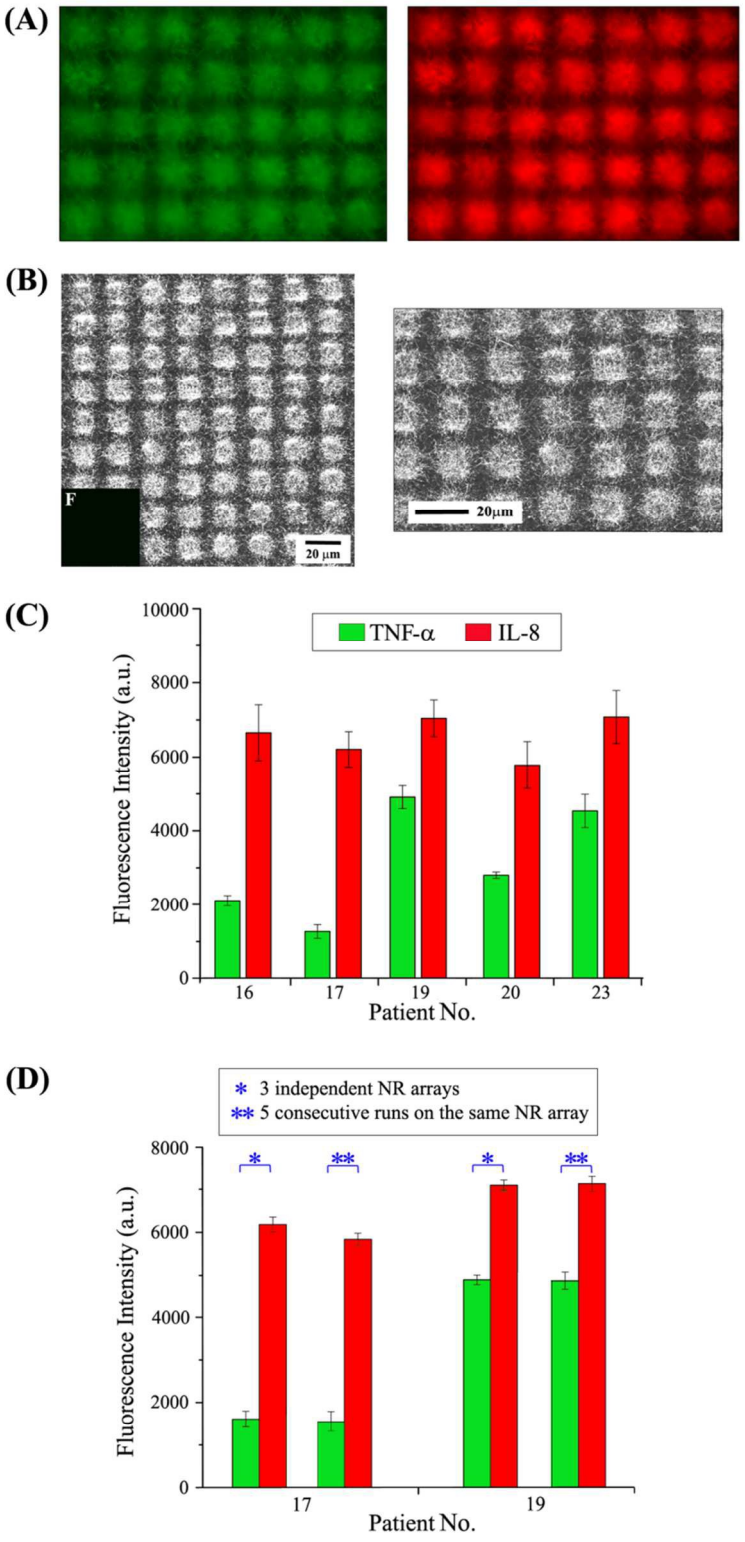

Figure 2. (A) The two fluorescence panels are representative emission data collected after performing the sandwich assays on the ZnO NRs against the patient samples and simultaneously measuring the protein concentrations. The left and right panels are the fluorescence signals corresponding to TNF-α and IL-8, respectively, from the patient No 24. **(B)** The SEM panels display the morphology and

dimensions of the square platforms of vertical ZnO NRs used in the fluorescence detection of TNF-α and IL-8. The inset in the left image, indicated as F, shows the fluorescence panel of the as-synthesized ZnO NR array probed with λ_{ex} = 450-490 nm. ZnO NRs exhibit no background fluorescence emission upon excitation at the wavelength ranges used to detect the proteins. **(C)** Exemplar fluorescence intensity plots from selected patients are presented to show the different amounts of TNF-α and IL-8 present in the urine. **(D)** The bar graphs display the variability in the fluorescence signals measured from repeated TNF-α and IL-8 assays of the same sample performed via the ZnO NRs-based method. In order to evaluate the inter- and intra-assay variability, TNF-α and IL-8 assays for the two selected patients (Nos 17 & 19) were carried out on three different ZnO NR arrays (data shown under *) as well as on the same ZnO NR array five consecutive times (data provided with **), respectively.

To assess the effectiveness of our ZnO NRs-based approach in simultaneously detecting the levels of TNF-α and IL-8 in patient urine samples, the concentrations obtained from the ZnO NR sandwich assays were compared directly to those determined in the same patient samples using commercially available ELISA kits. In order to make quantitative comparisons, calibration curves were generated for each protein using standard solutions containing known amounts of IL-8 and TNF-α. Fig. 3 displays the calibration curves for IL-8 and TNF-α obtained by the ELISA- and ZnO NRs-based assays. Figs. 3(A) and 3(B) are the standard curves of IL-8 and TNF-α, respectively, using commercially obtained ELISA kits. Per kit instructions, the calibration data points were fitted using a four-parameter nonlinear function whose fitting results were subsequently used to calculate the unknown IL-8 and TNF-α concentrations in patient samples. The DL of the ELISA-based method was 7.5 pg/mL for IL-8 and 5.5 pg/mL for TNF-α as defined by 2 standard deviations above the mean value for 20 zero concentration replicates. On the other hand, Figs. 3(C) and 3(D) correspond to the standard curves of

IL-8 and TNF-α, respectively, evaluated on the ZnO NR platforms. The regressions using the normalized fluorescence intensity versus the log-transformed protein concentrations yielded linear fits with adjusted coefficient of determination values as specified in each graph. On the ZnO NR platforms, DLs assessed via a methodology involving the upper boundary of blank samples measured in the absence of the measurand proteins[49] were 5.5 fg/mL for IL-8 and 4.2 fg/mL for TNF-α with a 95% accuracy goal. An alternative approach with the Hubaux-Vos methodology,[50] involving the linear calibration curves and the associated 95% confidence bands in Figs. 3(C and D), yielded DLs of 58.9 fg/mL for IL-8 and 39.8 fg/mL for TNF-α. DL estimations from the Hubaux-Vos methodology are typically reported to be higher than the previously described approach as calibration data deviate from the homoscedasticity hypothesis assumed throughout the range of concentrations used in the calibration.[51,52] Regardless of the methods used to estimate the biomarker detection capability, the DLs of the two different assay techniques reveal an unparalleled sensitivity down to several fg/mL for the ZnO NRs-based assay compared with several pg/mL for the ELISA assay.

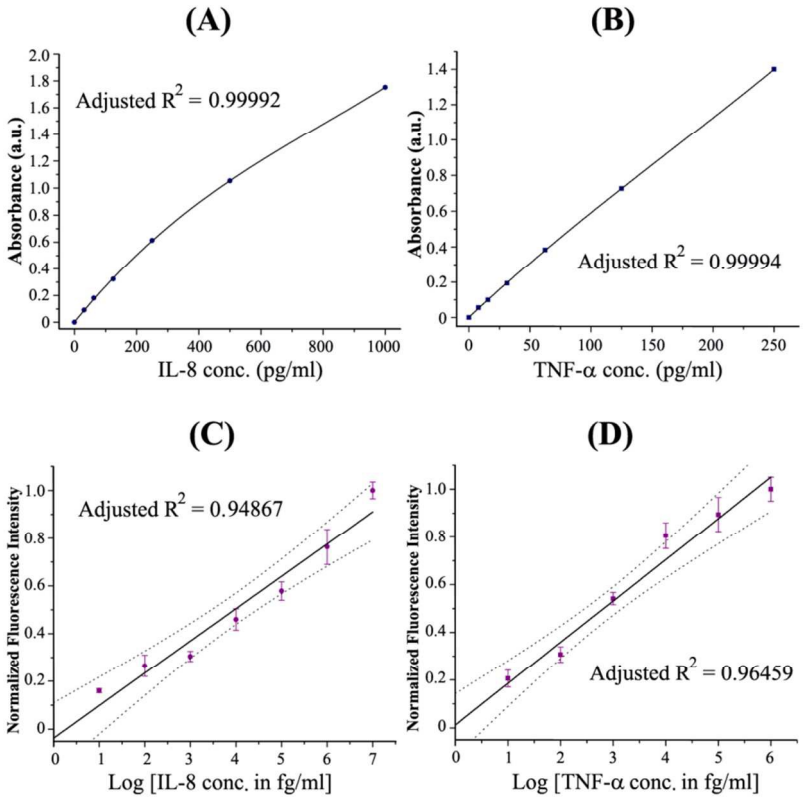

Figure 3. (A and B) Calibration curves of IL-8 and TNF-α produced by the ELISA method are displayed in panel (A) and (B), respectively. Absorbance readings from IL-8 and TNF-α standards were plotted against its concentration. The solid lines in the graphs are the 4-parameter fitting curves yielding the reported values of adjusted coefficient of determination (R^2). **(C and D)** Calibration curves for IL-8 and TNF-α established on the ZnO NR detection platform are shown in panel (C) and (D), respectively. The standard curves were generated by evaluating fluorescence intensities measured from known amounts of each protein. The solid black line in each graph corresponds to a linear fit through the data points with the indicated R^2 value. The dotted black lines indicate 95% confidence intervals.

IL-8 levels in the urine of 38 patients were measured by the ELISA- and ZnO NRs-based assays and the concentrations obtained by the two methods were compared for each patient. The 3-dimensional (3D) bar graphs in Fig. 4(A) display the patient IL-8 levels from the two techniques based on their respective calibration curves in Fig. 3. Urine IL-8 could be detected in all of the individuals with either the ELISA- or ZnO NRs-based method and ranged between several tens of pg/mL to a few ng/mL. The bar graphs in Fig. 4(B), plotted using an upper limit of 400 pg/mL, more clearly illustrate the agreement between the two methods for samples with lower IL-8 levels.

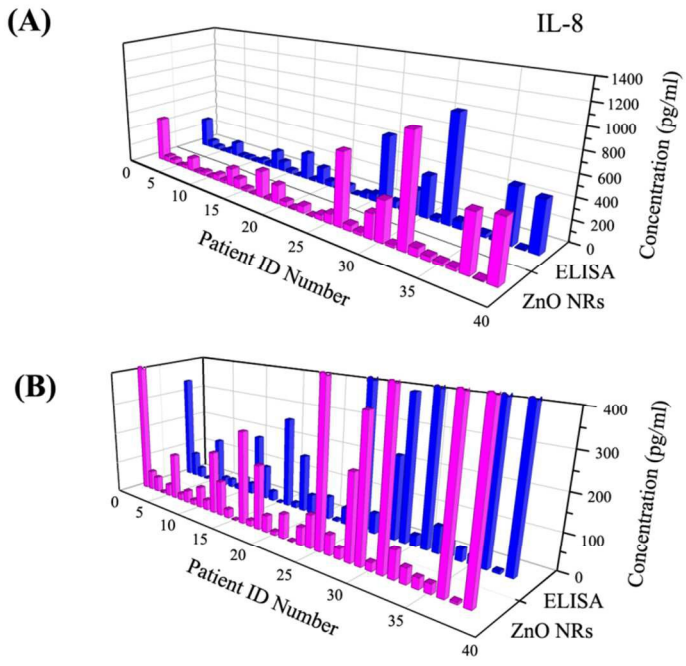

Figure 4. (A) The 3D bar graphs display the IL-8 concentrations in the patients' samples determined by using the ELISA- and ZnO NRs-based platforms. **(B)** In order to show the lower range data more clearly, the 3D bar graphs of the patients' IL-8 values from the two methods are compared by using the upper concentration limit of 400 pg/mL. The truncated bars indicate that the IL-8 levels exceed the upper limit of the 3D graph.

For additional quantitative comparison between the IL-8 results acquired by the ELISA and ZnO NR approaches, the readings were evaluated using the Bland-Altman analysis.[53] The results from the analysis are summarized in Fig. 5. The correlative plot in Fig. 5(A) displays the IL-8 readings from the same patients determined by the ELISA and ZnO NRs method on the x and y axis, respectively, as well as the linear fit of the data points shown as the dashed red line. The solid black line, signifying identical IL-8 readings from the two methods, is superimposed on the scatter plot as a guide to the eye. Our data points lie on or close to the guide line, indicating excellent agreement between the IL-8 values established by the two assay techniques. Additionally, the histogram distribution chart in Fig. 5(B) shows the number of samples exhibiting the various differences between the IL-8 concentrations using

each assay method. The majority of the IL-8 readings from the two methods fell within the range of ±2.5 pg/mL. The IL-8 concentrations obtained from the two methods were also compared by plotting the differences between the ELISA and ZnO NR readings versus the mean concentration values between the two techniques. The analyzed data centered near the black lines inserted in Figs. 5(C and D) whose traces represent equivalent IL-8 readings from the same patient when assayed by the two methods. Hence, based on these comparative IL-8 results, we demonstrate that the ZnO NR platform can be successfully employed for the accurate quantification of urinary biomarker proteins directly from patient samples.

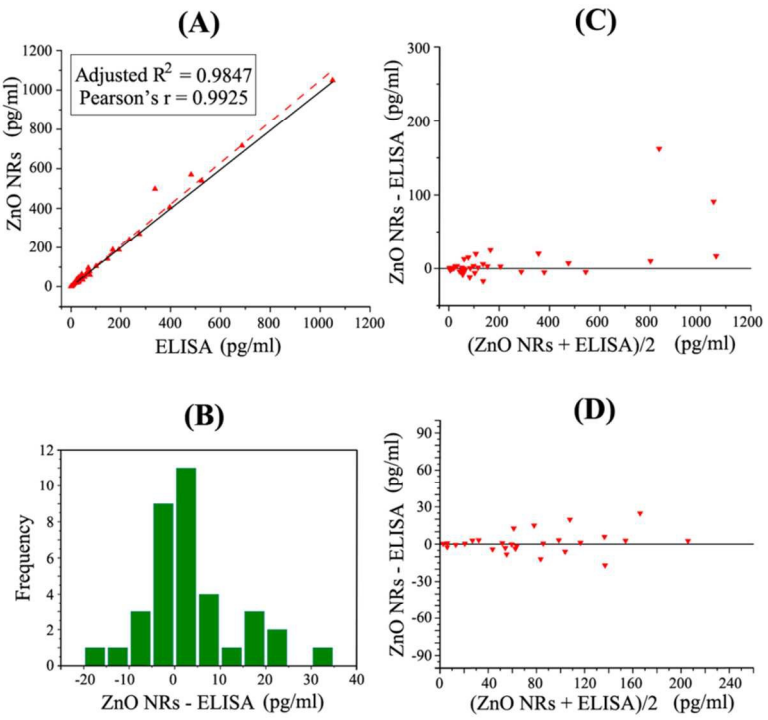

Figure 5. (A) The ELISA and ZnO NR assay results are directly compared from the same set of patients by plotting each patient's IL-8 reading in pg/mL evaluated by the different methods along the x (ELISA) and y (ZnO NRs) axis. The dashed red line is the linear fit through the data. The ELISA and ZnO NRs assay results fall on or near the black line of y = x, indicating good agreement between the

patient IL-8 values established by the two assay techniques. **(B)** The histogram distributions chart patient counts versus the differences in the evaluated IL-8 concentrations between the two assay techniques for the (ZnO NRs-ELISA) range of less than 40 pg/mL. The majority of the patients' IL-8 readings fall within the range of ±2.5 pg/mL from the reading of each technique. **(C)** The IL-8 concentrations in pg/mL determined from the ZnO NR and ELISA assays are compared by plotting the differences between the two techniques, (ZnO NRs-ELISA), on the y-axis and the means of the two techniques, (ZnO NRs + ELISA)/2, on the x-axis. The evaluated data lie close to the black line of y = 0 whose trace corresponds to equivalent readings of IL-8 concentrations in the two assays from the same patients. **(D)** The scatter plot shown in **(C)** is rescaled to clearly present the lower range data.

In order to substantiate the applicability of ZnO NRs-based platforms in ultrasensitive cytokine detection, comparative measurements of urine TNF-α were performed on samples from 46 individuals. The 3D bar graphs in Fig. 6 (A) summarize the TNF-α levels of each patient determined by the ELISA- and ZnO NRs-based assays. Many of the values were near or below the DL of the ELISA assay. The undetermined concentration data of these patients are marked as grey blocks in the ELISA row in Fig. 6(A). In contrast, urine TNF-α could be measured using the ZnO NR platforms in all patients, including those who could not be readily measured with the ELISA assay. These low-level samples are marked with the magnifier sign in the ZnO NR row of Fig. 6(A) and, are displayed on different scales in Fig. 6(B and C) for clarity. As also supported by these results, urine TNF-α values well below tens of pg/mL could be successfully measured by the ZnO NR technique. The demonstrated detection level suggests that the potential application of our ZnO NRs-based approach is not limited just to serving as an alternative or a tandem detection platform to an existing measurement method, but rather, its role can be extended to the much needed, ultrasensitive detection of biomarker proteins in samples below the concentration levels that standard techniques can ascertain.

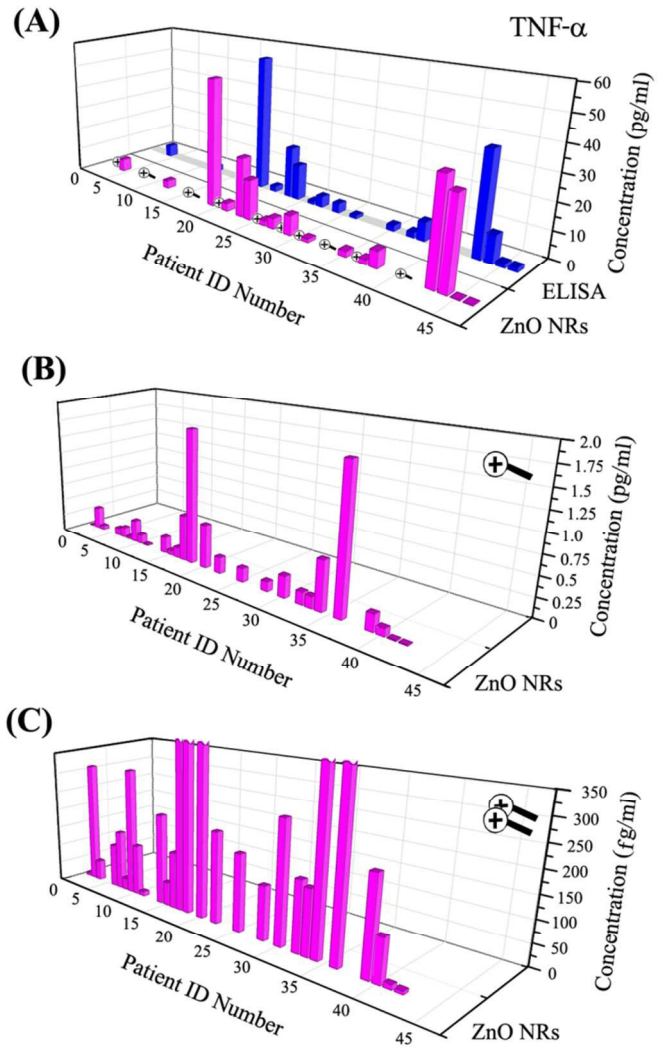

Figure 6. (A) The 3D bar graphs display the TNF-α concentrations in the urine samples measured by the ELISA- and ZnO NRs-based platforms for comparison. The grey regions in the ELISA row correspond to missing concentration data, indicating that the TNF-α levels in the samples were below the ELISA DL of 5.5 pg/mL. In contrast, ZnO NRs were able to measure TNF-α concentrations of all 46 patients. The magnifier signs inserted in the ZnO NRs row correspond to the patients that belong to the grey area of the ELISA-based assay, and the bar graphs of these patients are shown separately in (B and C) for clarity. **(B and C)** The zoomed-in 3D bar graphs are the missing TNF-α concentrations that were revealed by the ZnO NRs-based assay. The upper limits of the vertical ranges in (B) and (C) are

adjusted to 2 pg/mL and 350 fg/mL, respectively, in order to show the variations in the TNF-α concentrations between patients more clearly. The truncated bars indicate that their TNF-α concentrations exceed the upper limit of the 3D graph.

As a proof-of-principle, we examined whether quantitation of low levels of urine cytokines may have clinical value in detecting or predicting AKI. Specifically, we measured urine TNF-α levels in an additional set of 52 intensive care unit (ICU) patients using ZnO NRs-based assays and correlated them with the clinical diagnosis of kidney injury. Subjects were assigned to three categories: *no AKI* (stable kidney function throughout their ICU admission); *Day 1 AKI* (AKI was present within 24 h of admission to the ICU) and *ICU AKI* (AKI developed after the first 24 h of ICU admission). TNF-α levels of all 52 patients were successfully assayed on the ZnO NR platforms and the results are summarized in Fig. 7. The majority of these levels were below the DL of the ELISA assay. The data presented in Fig. 7 suggest that the typical range of the urine TNF-α concentrations in the *no AKI* group is below several hundreds of fg/mL whereas the TNF-α levels of the majority of patients associated with the *Day 1 AKI* group lie above a few pg/mL. The data from the patients in the *ICU AKI* category separate into two concentration blocks, one close to that of the *no AKI* and the other similar to that of the *Day 1 AKI* patients. Hence, the ZnO NR method may enable diagnostic or predictive use of urine TNF-α levels for clinical use by providing information that cannot be facilely deduced from conventional, lower sensitivity assays.

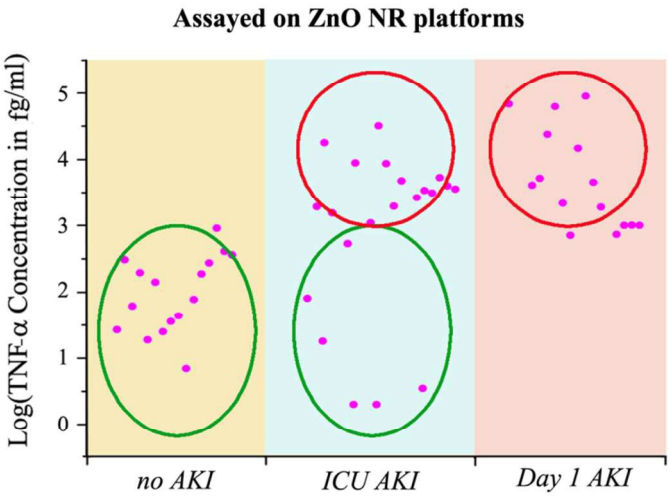

Figure 7. The scatter plots show the distribution patterns of TNF-α concentrations for subjects in the three different categories of *no AKI, ICU AKI*, and *Day 1 AKI*. The ZnO NR assay enables highly sensitive TNF-α detection of all patients. In addition, the characteristic distribution of the TNF-α concentration values associated with each AKI category can be identified, as indicated by the green and red circles in the graph.

The typical concentrations of IL-8 and TNF-α in healthy subjects are reported to be approximately in the range of 40 pg/mL and 5 pg/mL, respectively, in a study involving human serum samples.[54] In another study involving urine samples, the control (no AKI) group showed IL-8 and TNF-α levels of 1.5 pg/mL and 0.12 pg/mL, respectively, whereas these values changed significantly to 74 pg/mL and 14 pg/mL, respectively, for the test (AKI) group.[55] While these values are provided as a point of reference, it should be also noted that various factors such as the age, gender, ethnicity, simultaneous occurring health problems, and dates of sample collection can all affect the exact baseline levels of the proteins.

Our ZnO NRs-based approach presents several advantages compared with existing methods. Our ZnO NRs-based detection requires approximately 90 min of total assay time and 60 μL of total bioreagent/patient sample volume for a typical run, including the biomedical reaction steps and subsequent fluorescence measurements. The rapid time and low volume associated with the ZnO NRs-based detection can be beneficial in a clinical setting. Additional benefits of the ZnO NR approach include factors related to its automation and integration potential. Although the different square patches in the ZnO NR array platform were treated with the same patient sample per run in our assays, each square feature has a potential to serve as a discrete detection element when coupled with appropriate patient sample delivery and fluorescence readout mechanisms. Future automation strategies, involving the simultaneous robotic delivery of many samples onto different NR patches and multichannel fluorescence detection of multiple analytes labelled with different fluorophores, may increase the scalability of our methodology. As fluorescence is one of the most extensively utilized mechanisms to produce optical signals in biomedical and clinical detection, breakthrough technologies via seamless and integration-ready means have been long sought to promote rapid and ultrasensitive fluorescence detection. When considering this need, our demonstrated ZnO NRs-based approach may be particularly attractive since it offers increased fluorescence detection capability that can be readily attained without involving extensive alterations or improvements to existing fluorescence imaging instruments and array/plate readers. In addition, the NRs can be directly used after their synthesis through well-known growth methods[28-31,34-39] without any post-synthetic modifications. The spectroscopic property of the ZnO NRs, showing no absorption or emission in the visible wavelength range, prevents the detection platform from potentially interfering with the optical profiles of common fluorophores[56] used in biodetection. Furthermore, the ZnO NR plates are durable and sturdy enough to withstand the biological and chemical reaction environments of our assays directly involving patient samples. In our typical assay environment of urine samples, the ZnO NR platforms were confirmed to withstand at least 25 repeated uses. These advantages contribute to the potential utility of our ZnO NRs as a low-volume

and low-cost assay much needed in screening of clinically relevant samples. The promising results obtained using the ZnO NRs may be beneficial for the identification and development of additional biomarkers beyond the cytokine and chemokine examples presented in this study, especially in the early clinical profiling of low-abundance biomarker levels in physiological fluids.

Summary

In summary, we have demonstrated that ZnO NRs can be successfully employed in the rapid, ultrasensitive, quantitative, and simultaneous detection of multiple AKI-related biomarkers in patient urine. Using the model protein of IL-8 for an AKI-implicated chemokine, we validated and benchmarked the detection readouts and the performance parameters of our ZnO NRs-based fluorescence technique against a conventional ELISA-based method on the same patient samples. We further evaluated the full detection capability of the ZnO NRs-based technique by quantifying the amounts of another AKI-related cytokine, TNF-α, whose levels in urine are often below the DLs of conventional detection methods. We first established the DLs of the ZnO NRs-based platform to be in the several fg/mL range. We subsequently employed the technique for the reliable and repeated quantification of the low-expressed, hard-to-trace TNF-α concentrations in patient urine samples. We have also demonstrated the feasibility of using our ZnO NRs-based approach for differentiating cytokine concentration ranges in different patient groups and for serving as a potential guide for further clinical monitoring. The fact that the ultrahigh detection sensitivity can be conveniently and straightforwardly achieved from minimally processed patient samples suggests potentially exciting and useful applications of the presented ZnO NRs-based assay schemes both in basic biology research and clinical studies for early disease diagnosis and treatments. In conjunction with the other advantages of our ZnO NRs-based detection approach as detailed in the discussion section, its application may be readily extended to other biomarker systems in physiological samples, beyond the model proteins in this study.

Acknowledgement

The authors acknowledge financial support on this work by the National Institutes of Health, National Research Service Award (1R01DK088016) from the National Institute of Diabetes and Digestive and Kidney Diseases.

Footnote

†Electronic supplementary information (ESI) available: Typical SEM images of the ZnO NRs used in the biomarker assays are provided in Fig. S1.

References

1. V. R. Preedy and R. J. Hunter, *Cytokines*, CRC Press, Boca Raton, FL, 2011.
2. M. Feldmann, *J. Clin. Invest.*, 2008, **118**, 3533-3536.
3. R. N. Fichorova, N. Richardson-Harman, M. Alfano, L. Belec, C. Carbonneil, S. Chen, L. Cosentino, K. Curtis, C. S. Dezzutti, B. Donoval, G. F. Doncel, M. Donaghay, J.-C. Grivel, E. Guzman, M. Hayes, B. Herold, S. Hillier, C. Lackman-Smith, A. Landay, L. Margolis, K. H. Mayer, J.-M. Pasicznyk, M. Pallansch-Cokonis, G. Poli, P. Reichelderfer, P. Roberts, I. Rodriguez, H. Saidi, R. R. Sassi, R. Shattock and J. J. E. Cummins, *Anal. Chem.*, 2008, **80**, 4741-4751.
4. C. Nathan and M. Sporn, *J. Cell Biol.*, 1991, **113**, 981-986.
5. L. C. Borish and J. W. Steinke, *J. Allergy Clin. Immunol.*, 2003, **111**, S460-S475.
6. O. Kwon, B. A. Molitoris, M. Pescovitz and K. J. Kelly, *Am. J. Kidney Dis.*, 2003, **41**, 1074-1087.
7. O. Liangos, A. Kolyada, H. Tighiouart, M. C. Perianayagam, R. Wald and B. L. Jaber, *Nephron Clin. Pract.*, 2009, **113**, c148-c154.
8. G. Gao, B. Zhang, G. Ramesh, D. Betterly, R. K. Tadagavadi, W. Wang and W. B. Reeves, *Am. J. Physiol. Renal Physiol.*, 2013, **304**, F515-F521.
9. G. Ramesh and W. B. Reeves, *J. Clin. Invest.*, 2002, **110**, 835-842.
10. G. M. Chertow, E. Burdick, M. Honour, J. V. Bonventre and D. W. Bates, *J. Am. Soc. Nephrol.*, 2005, **16**, 3365-3370.
11. W. B. Reeves, O. Kwon and G. Ramesh, *Am. J. Physiol. Renal Physiol.*, 2008, **294**, F731-F738.
12. W. Wang, W. B. Reeves and G. Ramesh, *Am. J. Physiol. Renal Physiol.*, 2008, **294**, F739-F747.
13. W. F. Bobrowski, J. E. McDuffie, G. Sobocinski, J. Chupka, E. Olle, A. Bowman and M. Albassam, *Cytokine*, 2005, **32**, 194-198.
14. D. Amsen, K. E. de Visser and T. Town, *Methods Mol. Biol.*, 2009, **511**, 107-142.

15. E. Staples, R. J. M. Ingram, J. C. Atherton and K. Robinson, *J. Immunol. Methods*, 2013, **394**, 1-9.

16. J. A. Stenken and A. J. Poschenrieder, *Anal. Chim. Acta*, 2015, **853**, 95-115.

17. I. Vancurova, *Cytokine Bioassays*, Springer, New York, NY, 2014.

18. R. T. Carson and D. A. A. Vignali, *J. Immunol. Methods*, 1999, **227**, 41-52.

19. E. Morgan, R. Varro, H. Sepulveda, J. A. Ember, J. Apgar, J. Wilson, L. Lowe, R. Chen, L. Shivraj, A. Agadir, R. Campos, D. Ernst and A. Gaur, *Clin. Immunol.*, 2004, **110**, 252-266.

20. M. Adler, R. Wacker and C. M. Niemeyer, *Analyst*, 2008, **133**, 702-718.

21. L. Potůčková, F. Franko, M. Bambousková and P. Dráber, *J. Immunol. Methods*, 2011, **371**, 38-47.

22. D. Scott, E. Dikici, M. Ensor and S. Daunert, *Annu. Rev. Anal. Chem.*, 2011, **4**, 297-319.

23. B. Schweitzer, S. Roberts, B. Grimwade, W. Shao, M. Wang, Q. Fu, Q. Shu, I. Laroche, Z. Zhou, V. T. Tchernev, J. Christiansen, M. Velleca and S. F. Kingsmore, *Nat. Biotech.*, 2002, **20**, 359-365.

24. L. Yuan, X. Hua, Y. Wu, X. Pan and S. Liu, *Anal. Chem.*, 2011, **83**, 6800-6809.

25. T.-H. Chou, C.-Y. Chuang and C.-M. Wu, *Cytokine*, 2010, **51**, 107-111.

26. J. Martinez-Perdiguero, A. Retolaza, L. Bujanda and S. Merino, *Talanta*, 2014, **119**, 492-497.

27. C.-Y. Chiang, M.-L. Hsieh, K.-W. Huang, L.-K. Chau, C.-M. Chang and S.-R. Lyu, *Biosens. Bioelectron.*, 2010, **26**, 1036-1042.

28. V. Adalsteinsson, O. Parajuli, S. Kepics, A. Gupta, W. B. Reeves and J. Hahm, *Anal. Chem.*, 2008, **80**, 6594-6601

29. A. Dorfman, N. Kumar and J. Hahm, *Adv. Mater.*, 2006, **18**, 2685-2690.

30. A. Dorfman, N. Kumar and J. Hahm, *Langmuir*, 2006, **22**, 4890-4895.

31. N. Kumar, A. Dorfman and J. Hahm, *Nanotech.*, 2006, **17**, 2875-2881.

32. M. Singh, R. Jiang, H. Coia, D. S. Choi, A. Alabanza, J. Y. Chang, J. Wang and J.-i. Hahm, *Nanoscale*, 2015, **7**, 1424-1436.

33. M. Singh, S. Song and J.-i. Hahm, *Nanoscale*, 2014, **6**, 308-315.

34. Z. L. Wang, *ACS Nano*, 2008, **2**, 1987-1992.

35. Z. L. Wang, *J. Phys.: Condens. Matter*, 2004, **16**, R829.

36. P. X. Gao and Z. L. Wang, *J. Phys. Chem. B*, 2004, **108**, 7534-7537.

37. L. E. Greene, M. Law, D. H. Tan, M. Montano, J. Goldberger, G. Somorjai and P. Yang, *Nano Lett.*, 2005, **5**, 1231-1236.

38. L. E. Greene, M. Law, J. Goldberger, F. Kim, J. C. Johnson, Y. Zhang, R. J. Saykally and P. Yang, *Angew. Chem. Int. Ed.* , 2003, **42**, 3031-3034.

39. P. Yang, H. Yan, S. Mao, R. Russo, J. Johnson, R. Saykally, N. Morris, J. Pham, R. He and H. J. Choi, *Adv. Funct. Mater.*, 2002, **12**, 323-331.

40. R. L. Mehta, J. A. Kellum, S. V. Shah, B. A. Molitoris, C. Ronco, D. G. Warnock, A. Levin and the Acute Kidney Injury Network, *Crit. Care*, 2007, **11**, R31-R31.

41. D. Kalavrizioti, M. Gerolymos, M. Rodi, P. Kalliakmani, S. Provatopoulou, T. Eleftheriadis, A. Mouzaki and D. S. Goumenos, *Cytokine*, 2015, **76**, 260-269.

42. J. Sirota, A. Walcher, S. Faubel, A. Jani, K. McFann, P. Devarajan, C. Davis and C. Edelstein, *BMC Nephrol.*, 2013, **14**, 1-9.

43. B. H. Rovin, H. Song, D. J. Birmingham, L. A. Hebert, C. Y. Yu and H. N. Nagaraja, *J. Am. Soc. Nephrol.* , 2005, **16**, 467-473.

44. C. Zhang, F. Zhang, T. Xia, N. Kumar, J.-i. Hahm, J. Liu, Z. L. Wang and J. Xu, *Opt. Express*, 2009, **17**, 7893-7900.

45. J. Hahm, in *Metal-enhanced Fluorescence*, ed. C. D. Geddes, John Wiley & Sons, Inc., Hoboken, NJ, 2010, ch. 12, pp. 363-391.

46. D. J. Sirbuly, M. Law, P. Pauzauskie, H. Yan, A. V. Maslov, K. Knutsen, C.-Z. Ning, R. J. Saykally and P. Yang, *Proc. Natl. Acad. Sci. U.S.A*, 2005, **102**, 7800-7805.

47. M. Law, D. J. Sirbuly, J. C. Johnson, J. Goldberger, R. J. Saykally and P. Yang, *Science*, 2004, **305**, 1269-1273.

48. V. A. Semenova, J. Schiffer, E. Steward-Clark, S. Soroka, D. S. Schmidt, M. M. Brawner, F. Lyde, R. Thompson, N. Brown, L. Foster, S. Fox, N. Patel, A. E. Freeman and C. P. Quinn, *J. Immunol. Methods*, 2012, **376**, 97-107.

49. S. Huang, T. Wang and M. Yang, *Assay Drug Dev. Technol.*, 2013, **11**, 35-43.

50. R. D. Gibbons and D. E. Coleman, *Statistical Methods for Detection and Quantification of Environmental Contamination*, John Wiley & Sons Inc., New York, NY, USA, 2001.

51. A. Hubaux and G. Vos, *Anal. Chem.*, 1970, **42**, 849-855.

52. L. J. J. Catalan, V. Liang and C. Q. Jia, *Journal of Chromatography A*, 2006, **1136**, 89-98.

53. D. G. Altman and J. M. Bland, *J. R. Soc. Series D (The Statistician)* 1983, **32**, 307-317.

54. A. Biancotto, A. Wank, S. Perl, W. Cook, M. J. Olnes, P. K. Dagur, J. C. Fuchs, M. Langweiler, E. Wang and J. P. McCoy, *PLoS ONE*, 2013, **8**, e76091.

55. O. Kwon, K. Ahn, B. Zhang, T. Lockwood, R. Dhamija, D. Anderson and N. Saqib, *Renal Failure*, 2010, **32**, 699-708.

56. J. R. Lakowicz, *Principles of Fluorescence Spectroscopy*, Springer, New York, NY, USA, 2006.

TOC Graphics

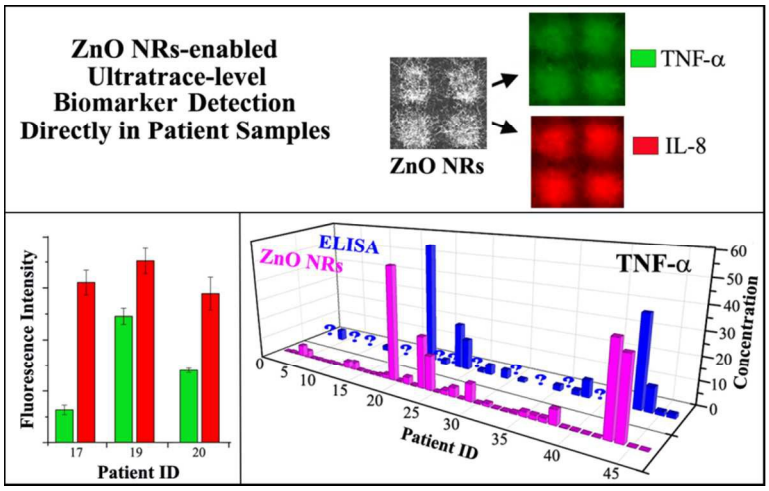

A ZnO NRs-based approach is employed in the rapid, quantitative, and simultaneous detection of multiple biomarkers directly in patient samples, providing an unparalleled detection capability beyond those of conventional methods.